

# DETECTION OF THE 62 $\mu$ m CRYSTALLINE H<sub>2</sub>O ICE FEATURE IN EMISSION TOWARD HH 7 WITH ISO-LWS<sup>0</sup>

SERGIO MOLINARI

Infrared Processing and Analysis Center, California Institute of Technology, MS 100-22, Pasadena, CA 91125, USA  
 CECILIA CECCARELLI

Laboratoire d'Astrophysique, Observatoire de Grenoble - BP 53, F-38041 Grenoble cedex 09, France  
 GLENN J. WHITE

Department of Physics, Queen Mary and Westfield College, University of London, Mile End Road, London E1 4NS, UK  
 Stockholm Observatory, S-133 36 - Saltsjöbaden, Sweden  
 PAOLO SARACENO

CNR-Istituto di Fisica dello Spazio Interplanetario, Area di Ricerca Tor Vergata, via Fosso del Cavaliere I-00133 Roma, Italy  
 BRUNELLA NISINI AND TERESA GIANNINI  
 Osservatorio Astronomico di Roma, via Frascati 33, I-00044 Monte Porzio, Italy  
 EMMANUEL CAUX  
 CESR CNRS-UPS, BP 4346, F-31028 Toulouse Cedex 04, France

*Draft version August 19, 2013*

## ABSTRACT

We report the detection of the 62  $\mu$ m feature of *crystalline* water ice in emission towards the bow-shaped Herbig-Haro object HH 7. Significant amounts of far infrared continuum emission are also detected between 10 and 200  $\mu$ m, so that Herbig-Haro objects cease to be pure emission-line objects at FIR wavelengths. The formation of crystalline water ice mantles requires grain temperatures  $T_{gr} \gtrsim 100$  K at the time of mantle formation, suggesting that we are seeing material processed by the HH 7 shock front. The deduced ice mass is  $\sim 2 \times 10^{-5} M_{\odot}$  corresponding to a water column density  $N(H_2O) \sim 10^{18} \text{ cm}^{-2}$ ; an estimate of the  $[H_2O]/[H]$  abundance yields values close to the interstellar gas-phase oxygen abundance. The relatively high dust temperature and the copious amounts of gas-phase water needed to produce the observed quantity of crystalline water ice, suggest a scenario where both dissociative and non-dissociative shocks co-exist. The timescale for ice mantle formation is of the order of  $\sim 400$  years, so that the importance of gas-phase water cooling as a shock diagnostic may be greatly diminished.

*Subject headings:* (ISM:) dust, extinction — ISM: Herbig-Haro objects — ISM: individual (HH 7) — ISM: lines and bands — infrared: ISM: continuum — infrared: ISM: lines and bands

## 1. INTRODUCTION

Herbig-Haro objects (HH; Haro 1950, Herbig 1951) are emission-line objects acting as signposts for the shock regions (Draine, Roberge & Dalgarno 1983; Hollenbach & McKee 1989) originating at the interface between stellar winds accelerated by Young Stellar Objects (YSOs) and the circumstellar or cloud ambient material. The temperature of dust grains in these shock regions can raise to only a few hundred degrees at most in dissociative shocks (Hollenbach & McKee 1989), so that their thermal emission cannot be detected below 10  $\mu$ m.

The instruments on board the *Infrared Space Observatory* satellite (ISO, Kessler et al. 1996) opened unprecedented possibilities for far infrared continuum studies of cold objects, including HH objects. In this *Letter* we present the data obtained with the Long (LWS, Clegg et al. 1996) and Short (SWS, de Graauw et al. 1996) Wavelength Spectrometer towards HH 7, the leading bow-shaped shock of the HH 7-11 chain emanating from the YSO SVS13, in the star forming region NGC 1333 in Perseus (d=350 pc). Details about the observations and data reduction are given elsewhere (Molinari et al. 1999). In Sect. 2 the additional data analysis procedures we adopted to derive a reliable continuum spec-

trum for HH 7 are discussed. Nomenclature for the ten LWS detectors is described in the ISO Data User Manual ([http://www.iso.vilspa.esa.es/manuals/lws\\_idum5](http://www.iso.vilspa.esa.es/manuals/lws_idum5)); detectors SW1 to SW5 (43-90  $\mu$ m), and LW1 to LW5 (80-197  $\mu$ m), are sometimes referred to as “short” and “long” wavelength detectors respectively.

## 2. RESULTS

The LWS beam centered on HH 7, also includes object HH 8 somewhat 20'' off-axis and HH 10 at the edge of the beam; these objects are however fainter than HH 7 at 2  $\mu$ m (Molinari et al. 1999) and the beam profile suppresses their possible contribution even more. Apart from a contamination by the strong nearby source SVS 13, which will be discussed in detail in Sect. 2.2, it is plausible to assume that HH 7 dominates the observed spectrum.

### 2.1. The 62 $\mu$ m feature

In Fig. 2.1 the complete spectra observed towards HH 7 and SVS 13 are shown. A broad feature extending from roughly 50 to 70  $\mu$ m is clearly visible in the HH 7 spectrum. For clarity the SW3 detector spectrum, with an offset applied to align it with the continuum of the adjacent detectors, is shown with plus symbols. The pri-

<sup>0</sup>Based on observations with ISO, an ESA project with instruments funded by ESA Member States (especially the PI countries: France, Germany, the Netherlands and the United Kingdom) with the participation of ISAS and NASA.

mary concern was to make sure that the 50-70  $\mu\text{m}$  feature was not a result of a residual instrumental effect and that it is intrinsic to HH 7. The passband calibration is known to be somewhat inaccurate for detector SW1 (it may be worse than 50% both in absolute and relative terms) which is the most sensitive to transients. Detectors SW2, SW3 and SW4 however, are stable in relative (passband) terms and a conservative figure of 30% can be assumed for their absolute calibration accuracy. The possibility that the broad feature visible on Fig. 2.1 may be due to the near-IR leaks present in the LWS detectors filters ([http://isowww.estec.esa.nl/notes/lws\\_0197.html](http://isowww.estec.esa.nl/notes/lws_0197.html)) can also be excluded. Finally, this feature might result from contamination effects from the bright nearby source SVS 13, which is the candidate exciting source for HH 7; these effects will be discussed in detail in the Sect. 2.2.

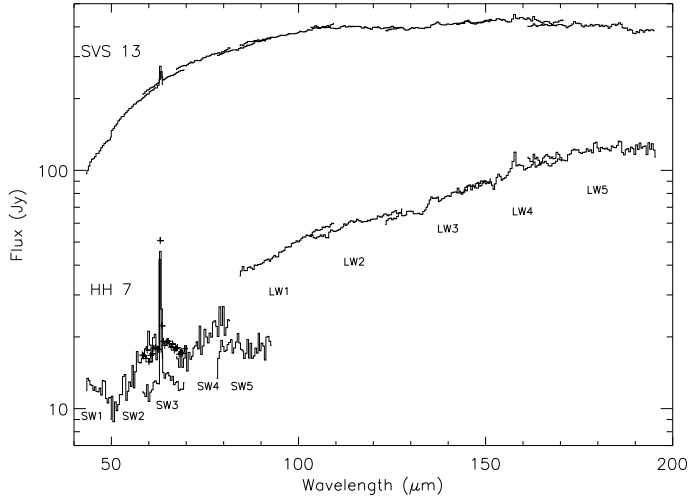


Fig. 1 – LWS averaged spectra observed towards HH 7 (bottom) and SVS 13 (top). The different portions are the 10 LWS detectors, labeled with the names used in the text. The plus symbols for HH 7 represent detector SW3 with an applied offset of 5 Jy to bring it in line with the adjacent detectors.

Here we just note here that if the 50-70  $\mu\text{m}$  feature seen on the HH 7 spectrum was due to a fraction of the flux emitted by the nearby contaminating source SVS 13, we would expect to see the same feature at a comparable “line-to-continuum” ratio on the SVS 13 continuum spectrum; Fig. 2.1 clearly shows that this is not the case. We conclude that the 50-70  $\mu\text{m}$  feature is real and intrinsic to HH 7 and we consider it as a  $2\sigma$  detection, assuming that the noise of the feature is equal to half the gap between detectors SW3 and SW2. We identify this as the 62  $\mu\text{m}$  feature due to the longitudinal acoustic modes of crystalline water ice (Bertie, Labbe & Whalley 1969), observed for the first time by Omont et al. (1990) in the expanding envelopes of post-AGB stars; ISO-LWS has detected this feature in the spectra of similar objects (Barlow 1998) and of a few Herbig Ae/Be stars (Waters & Waelkens 1998, Malfait et al. 1999). It is the first time this feature has been detected towards Herbig-Haro objects.

## 2.2. The 2-200 $\mu\text{m}$ Continuum

Several SWS line scans were used to estimate the continuum at different wavelengths for  $\lambda < 40 \mu\text{m}$ . The line-free portions of each individual spectrum were used to build

flux histograms, and a gaussian was then fitted to the core of the distribution to obtain the centroid (average flux) and the standard deviation; the latter was then divided by the square root of the number of points in histogram to get an estimate of the uncertainty. These uncertainties reflect the internal accuracy of the estimates; infact the true uncertainty may be higher. In particular, all data shortward of  $\sim 10 \mu\text{m}$  are at the detection limit of the SWS and they will be treated as  $1\sigma$  upper limits.

LWS scans were averaged using the ISO Spectral Analysis Package (ISAP, <http://www.ipac.caltech.edu/iso/isap/isap.html>) using a median clipping algorithm which rejected outlying data points due to incomplete removal of glitches from cosmic rays hits. However, contamination effects in the HH 7 spectrum due to the nearby ( $\sim 70''$  NW) candidate exciting source SVS 13 must be taken into account to assess if the observed continuum (Fig. 2.1 is all due to HH 7; for this purpose we used an irregularly sampled raster map of Mars taken as part of the LWS calibration programme. We first used the LIA (<http://www.ipac.caltech.edu/iso/lia/lia.html>) routine INSPECT\_RASTER to determine the relative position of HH 7 and SVS 13 in the [Y,Z] spacecraft frame of reference. For each Mars raster position along the direction connecting the two sources, we averaged the Mars spectra detector by detector; each detector average at the various off-axis positions was then ratioed to the analogue detector average of the on-axis spectra, and a set of ten contamination factors for each position was obtained. A spline interpolation was then used to estimate these factors (one per detector) at an off-axis distance of 68'', the distance between HH 7 and SVS 13; we find values 0.024, 0.025, 0.037, 0.05, 0.075, 0.09, 0.10, 0.11, 0.13 and 0.15, which increase with wavelength as expected due to diffraction. We multiplied the observed SVS 13 spectra by these numbers, and the resultant spectrum was subtracted from the observed HH 7 spectrum.

This method for estimating the contamination from nearby sources inevitably suffers from the irregular sampling of the Mars raster map. Raster points did not lay exactly along the HH 7-SVS 13 direction on the focal plane, and the interpolation between the correction factors estimated at each relevant raster position introduced an additional uncertainty. At the end of the procedure (see Fig. 3) we find worse alignment between adjacent LW detectors, and detector SW5 goes to negative flux values (not reported on Fig. 3). We believe this may be due to the fact that as the magnitude of the applied contamination correction increases with wavelength, so it does the associated uncertainty; in particular, detector SW5 is in the critical region where the contamination correction starts to be high (2-3 times higher than for SW2 and SW4) while the observed signal is still low (similar to SW2), so that a slightly overestimate of the contamination fraction is enough to bring its corrected values below zero. The LWS LW detectors are those for which the contamination fractions are higher and for which diffraction and source’s extension effects (which here have been neglected) are more severe. An additional complication, which does not affect the SW detectors, is that heavy fringing is observed (which has been here removed using standard tools available in ISAP); this has the effect of modulating the

beam size as a function of wavelength even within individual detector bands. We did not take this into account, instead deriving a single contamination factor per detector; multiplying or dividing by a constant, however, has the effect of changing the slope. Hence, although the observed continuum levels are high enough to ensure that an important part of the observed signal can confidently be assigned to HH 7, the exact absolute fluxes and spectral shape in this wavelength range remain highly uncertain.

On the short wavelength side of the LWS spectrum on the other hand, the existence of intrinsic continuum emission from HH 7 depends more critically on the particular value of the contamination factors; doubling this factors would lower the spectrum to negative flux levels. If, however, the  $\lambda \leq 80 \mu\text{m}$  flux observed towards HH 7 were due to contamination, we would expect to see the  $62 \mu\text{m}$  emission feature also on the continuum spectrum of SVS 13 and with a comparable “line/continuum”; instead, no trace of such a feature is seen on the SVS 13 continuum (see Fig. 2.1). We conclude that FIR emission which is intrinsic to HH 7 has been detected, showing for the first time that Herbig-Haro objects cease to be exclusively emission-line objects at FIR wavelengths.

### 3. DISCUSSION

In the following discussion we will assume that the FIR and mm continuum arise from the same region of space, based on the spatial coincidence between the HH objects and the mm emission distribution; currently available 50–100  $\mu\text{m}$  data on the region (Harvey et al. 1984, 1998; Jennings et al. 1987) however, do not have enough spatial resolution or sensitivity to support this claim.

The spectral energy distribution (SED) from HH 7 will be modeled as thermal emission from dust grains composed of a silicate core and a water ice mantle. Absorptivities between 2 and 300  $\mu\text{m}$  were computed with Mie theory in the formulation of Wickramasinghe (1967), using the complex refractive indices for crystalline water ice (Bertie et al. 1969) and silicate (Draine 1985). Longward of 300  $\mu\text{m}$  the silicate absorptivities by Draine (1985) were adopted; inclusion of water ice mantles may steepen the slope of the  $Q_{abs}$  vs  $\lambda$  relationship (Aannestad 1975), possibly leading to underestimation of the dust mass. Radiative transfer is approximated with an analytical treatment where dust is distributed on a sphere which is characterised by radial density and temperature gradients (Noriega-Crespo, Garnavich & Molinari 1998). The presence of a cold dust clump centered on the location of HH 7 and extending over a larger area than the one traced by the optical or near-IR emission (Lefloch et al. 1998), justifies a treatment where a dust clump is centrally heated by the HH 7 shock. Fig. 3 presents the complete SED towards HH 7, after removal of the contamination from SVS 13 (see Sect. 2.2). The LWS detectors SW1 to SW4 have been rescaled to a common level preserving their original mean value; no other rescaling was made to the rest of the LWS spectra. The continuum points from the SWS spectra and an estimate for the 1.25 mm flux integrated on the model fit area (see below) are also reported; the latter point has to be considered an upper limit since it is contaminated by SVS 13 just in the same way it happens for the LWS observations. We find that it is impossible to globally fit

the observed SED; considering the discussion in Sect. 2.2, we then decided to give higher priority to the short wavelength LWS detectors spectra also because these are the ones showing the  $62 \mu\text{m}$  feature, and more closely match each other (not considering the applied rescaling).

While the overall appearance of the continuum depends on the radius of the dust clump, its mass and temperature gradient, the “line/continuum” ratio of the  $62 \mu\text{m}$  feature depends on the relative size of the ice mantle with respect to the grain core. The  $62 \mu\text{m}$  water ice feature is well fitted by adopting a core radius of  $0.07 \mu\text{m}$  and a total core + mantle radius of  $0.1 \mu\text{m}$ . The model also suggests that the short wavelength end of the LWS spectrum can be identified with one side of the  $45 \mu\text{m}$  water ice feature (see also Dartois et al. 1998), also in emission; although detector SW1 is the one that experiences the most severe problems in calibration-related aspects, the further agreement of the model with the  $\lambda \sim 38.4 \mu\text{m}$  SWS point makes this a plausible possibility. The importance of the detection of the  $62 \mu\text{m}$  feature is that it is specific to crystalline water ice, as opposed to the  $45 \mu\text{m}$  feature which is instead predicted for both crystalline and amorphous ice (e.g. Moore et al. 1994). Most of the laboratory studies (e.g., Smith et al. 1994 and references therein) show that ice deposited onto grains at  $T \lesssim 100 \text{ K}$  is in amorphous state (but see Moore et al. 1994 who instead obtain crystalline ice in these conditions) also for deposition rates as high as  $20 \mu\text{m h}^{-1}$  (Léger et al. 1983); the  $62 \mu\text{m}$  feature is then an important indicator of the thermal history of the grains because it appears at  $T \gtrsim 100 \text{ K}$  when an irreversible transition from amorphous to crystalline state commences.

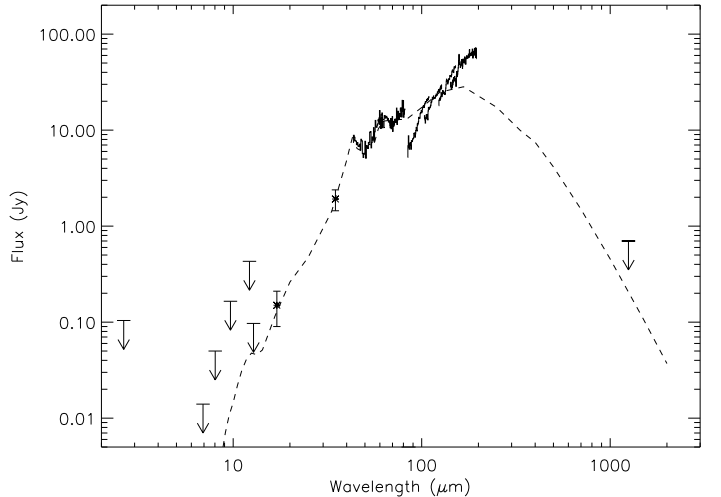


Fig. 2 – Complete spectral energy distribution towards HH 7. The full lines represent the LWS spectra after applying the contamination corrections discussed in the text. Detectors SW1 to SW4 have been rescaled to a common level preserving their original mean value.

The fit plotted in Fig. 3 is obtained adopting a dust clump radius of 0.06 pc, which approximates the radius of the average LWS beam size at a distance of 350 pc, and the size of the 1.25 mm continuum emission area (Lefloch et al. 1998). The density is assumed constant and equal to  $6 \times 10^{-4} \text{ cm}^{-3}$  while the temperature varies from  $\sim 10$  to 200 K with a  $\sim -0.4$  power-law radial gradient. The

bolometric luminosity obtained integrating the model fit is  $L_{fit} = 3.7 \text{ L}_\odot$ , while integration of the contamination-corrected SED (Sect. 2.2) yields  $L_{sed} \lesssim 4.5 \text{ L}_\odot$  (since  $\lambda < 10 \mu\text{m}$  and  $\lambda = 1.25 \text{ mm}$  data are to be considered upper limits); this is about a factor 30 higher than the cooling via atomic and molecular lines observed towards HH 7 (Molinari et al. 1999). The fitted model predicts that the bulk of the 62  $\mu\text{m}$  feature is emitted by dust at temperatures  $T \gtrsim 30 \text{ K}$  concentrated inside a 4''-radius region centered on HH 7, a size comparable to that of the optical and near-IR emission which traces the shock front. Since these grains should have experienced a rise in temperature to values  $\gtrsim 100 \text{ K}$  in order for ice mantles to be in crystalline state, it is plausible that **the 62  $\mu\text{m}$  feature originates from dust which has been processed by the HH 7 shock**. The dust mass in the 4''-radius region centered on HH 7 amounts to  $5 \times 10^{-5} \text{ M}_\odot$  (the total dust mass implied by the model fit is  $\sim 0.035 \text{ M}_\odot$ ); the relative proportion of core and mantle (the core has 70% of the total grain radius) implies a water ice mass of  $2 \times 10^{-5} \text{ M}_\odot$ , or a  $\text{H}_2\text{O}$  column density  $\sim 1.1 \times 10^{18} \text{ cm}^{-2}$ .  $\text{H}_2$  pure rotational lines (Molinari et al. 1999) suggest  $N(\text{H}_2) \sim 4.4 \times 10^{20} \text{ cm}^{-2}$  in the same 4''-radius region, implying  $[\text{H}_2\text{O}]/[\text{H}] \sim 1.25 \times 10^{-3}$ , or a factor  $\sim 4$  higher than the interstellar O gas-phase abundance (Meyer et al. 1998). However, this number should be regarded as an upper limit because our model assumes that *all* dust grains are coated with ice mantles, which is not necessarily true; besides, we cannot exclude the presence of cold  $\text{H}_2$  ( $T \lesssim 100 \text{ K}$ ) which our ISO observations (Molinari et al. 1999) would not trace. This water abundance, even if considered only as an order-of-magnitude estimate, is however much higher than the gas phase water abundance ( $[\text{H}_2\text{O}]/[\text{H}] \lesssim 10^{-5}$ ) deduced from FIR lines (Molinari et al. 1999), and it would essentially imply that most of the oxygen is locked into water ice.

Due to the uncertainty about the 45  $\mu\text{m}$  feature (see above), it hard to tell from the observational viewpoint whether gas-phase water produced behind the HH 7 shock front (Kaufman & Neufeld 1996) is deposited onto bare warm grains, or pre-existing ice mantles are warmed-up during the passage of a relatively gentle shock front. The ice optical constants that we used (Bertie et al. 1969) are from laboratory samples obtained by direct deposition at  $T=173 \text{ K}$  and subsequent cooling to 100 K; hence the good simultaneous fit of the 62 and 45  $\mu\text{m}$  features would tend to support the first scenario. The physical condition behind low velocity ( $v_s \lesssim 40 \text{ km s}^{-1}$ ), non-dissociative, shocks are favourable for the rapid gas-phase incorpora-

tion of atomic oxygen into water (Draine, Roberge & Dalgarno 1983, Kaufman & Neufeld 1996). Subsequent freezing onto grains (Bergin, Neufeld & Melnick 1998, 1999) in the cooling post-shock region could produce the observed water ice mantles, also explaining the minor role played by gas-phase water in the cooling of the HH 7 shock (Molinari et al. 1999). However, non-dissociative shocks are unable to raise the grain temperature to the  $T \gtrsim 100 \text{ K}$  (Draine, Roberge & Dalgarno 1983) needed to explain the presence of crystalline ice mantles; a dissociative component, whose generated intense UV field (Hollenbach & McKee 1989) is much more efficient in heating the grains, is needed. The co-existence of both types of shock is indeed an expected feature of bow shocks like HH 7 (Smith & Brand 1990) and it is independently supported by FIR lines studies (Molinari et al. 1999). However, we point out that this relies on the general result that crystalline ice requires relatively high temperatures to form; if crystalline ice can also form at low ( $T < 20 \text{ K}$ ) temperature (Moore et al. 1994) then a dissociative shock component may not be needed.

The alternative possibility that pre-existing amorphous water ice mantles are heated up during the passage of the shock front seems unlikely since the mantles are easily destroyed by grain-grain collisions once the shock velocities exceed  $\sim 15 \text{ km s}^{-1}$  (Caselli, Hartquist & Havnes 1997).

We can derive an order-of-magnitude estimate for the timescale  $\tau_{ice}$  of the formation of water ice mantles, dividing the linear size of the post-shock region by the shock velocity; assuming a maximum shock velocity of  $\sim 40 \text{ km s}^{-1}$  for the HH 7 shock (Solf & Böhm 1987, Molinari et al. 1999) and a linear extent of  $\sim 10''$  for the HH 7 post-shock region as estimated from  $\text{H}_2$  2.12  $\mu\text{m}$  images (Garden et al. 1990, Everett 1997, Molinari et al. 1999), we estimate  $\tau_{ice} \sim 400 \text{ yrs}$ , a factor  $\sim 250$  less compared to theoretical predictions for ice mantles formation behind non-dissociative shocks (Bergin, Neufeld & Melnick 1999). This very short timescale for ice mantle formation would make the gas-phase water cooling practically irrelevant as a shock diagnostic.

**Acknowledgements:** We thank B. Swinyard for providing us with the calibrated data for the Mars raster map we used to estimate the contamination corrections, and B. Lefloch for providing us with the integrated flux from his published 1.25 mm map of NGC 1333. We also thank A. Noriega-Crespo and E. Sturm for sharing their insight in SWS data. The ISO Spectral Analysis Package (ISAP) is a joint development by the LWS and SWS Instrument Teams and Data Centers. Contributing institutes are CESR, IAS, IPAC, MPE, RAL and SRON.

## REFERENCES

Aannestad, P.A. 1975, ApJ, 200, 30  
 Barlow, M.J. 1998, Ap&SS, 255, 315  
 Bergin, E.A., Neufeld, D.A., Melnick, G.J. 1998, ApJ, 499, 777  
 Bergin, E.A., Neufeld, D.A., Melnick, G.J. 1999, ApJ, 510, 145  
 Bertie, J.E., Labbe, H.J., Whalley, E. 1969, J. Phys. Chem., 50, 4501  
 Caselli, P., Hartquist, T.W., Havnes, O. 1997, A&A, 322, 296  
 Clegg, P.E., Ade, P.A.R., Armand, C., et al. 1996, A&A, 315, L38  
 Dartois, E., Cox, P., Roelfsema, P.R., et al. 1998, A&A, 338, L21  
 de Graauw, T., Haser, L.N., Beintema, D.A., et al. 1996, A&A, 315, L49  
 Draine, B.T. 1985, ApJS, 57, 587  
 Draine, B.T., Roberge, W.G., Dalgarno, A. 1983, ApJ, 264, 485  
 Everett, M.E. 1997, ApJ, 478, 246  
 Garden, R.P., Russel, A.P.G., Burton, M.G. 1990, ApJ, 354, 232  
 Haro, G. 1950, AJ, 55, 72  
 Harvey, P.M., Wilking, B.A., Joy, M. 1984, ApJ, 278, 156  
 Harvey, P.M., Smith, B.J., Di Francesco, J., Colomè, C. 1998, ApJ, 499, 294  
 Herbig, G.H. 1951, ApJ, 113, 697  
 Hollenbach, D., McKee, C.F. 1989, ApJ, 342, 306  
 Jennings, R.E., Cameron, D.H.M., Cudlipp, W., Hirst, C.J. 1987, MNRAS, 226, 461  
 Kaufman, M.J., Neufeld, D.A. 1996, ApJ, 456, 611  
 Kessler, M.F., Steinz, J.A., Anderegg, M.E., et al. 1996, A&A, 315, L27  
 Lefloch, B., Castets, A., Cernicharo, J., et al. 1998, A&A, 334, 269  
 Léger, A., Gauthier, S., Défourneau, D., Rouan, D. 1983, A&A, 117, 164

Malfait, K., Waelkens, C., Bouwman, J., De Koter, A., Waters, L.B.F.M. 1999, A&A, in press

Meyer, D.M., Jura, M., Cardelli, J.A. 1998, ApJ, 493, 222

Molinari, S., et al. 1999, in preparation

Moore, M.H., Ferrante, R.F., Hudson, R.L., et al. 1994, ApJ, 428, 81

Noriega-Crespo, A., Garnavich, P., Molinari, S. 1998, AJ, 116, 1388

Omont, A., Modeley, S.H., Forveille, T., et al. 1990, ApJ, 355, L27

Smith, M.D., Brand, P.W.J.L. 1990, MNRAS, 245, 108

Smith, R.G., Robinson, G., Hyland, A.R., et al. 1994, MNRAS, 271, 481

Solf, J., Böhm, K.H. 1987, AJ, 93, 1172

Waters, L.B.F.M., Waelkens, C. 1998, ARA&A, 36, 233

Wickramasinghe, N.C. 1967, "Interstellar Grains", Chapman & Hall eds., London